Near-surface weakening in Japan after the 2011 Tohoku-Oki earthquake

N. Nakata[1] and R. Snieder[2]

N. Nakata, Department of Urban Management, Kyoto University, Kyotodaigaku-Katsura, Nishikyo-ku, Kyoto, 615-8540, Japan. Center for Wave Phenomena, Department of Geophysics, Colorado School of Mines, 1500 Illinois Street, Golden, CO 80401, USA. (n_nakata@earth.kumst.kyoto-u.ac.jp)

R. Snieder, Center for Wave Phenomena, Department of Geophysics, Colorado School of Mines, 1500 Illinois Street, Golden, CO 80401, USA.

[1]Department of Urban Management, Kyoto University, Kyoto, Japan. Center for Wave Phenomena, Department of Geophysics, Colorado School of Mines, Golden, Colorado, USA.

[2]Center for Wave Phenomena, Department of Geophysics, Colorado School of Mines, Golden, Colorado, USA.

The magnitude (M_W) 9.0 Tohoku-Oki earthquake on 11 March 2011 was one of the largest in recent history. Ground motion caused by the seismicity around the time of the main shock was recorded by *KiK-net*, the strong-motion network that covers most of Japan. By deconvolving waveforms generated by earthquakes that are recorded at the surface and in a borehole at KiK-net station FKSH18, we detect a reduction of shear-wave velocity in the upper 100 m of about 10%, and a subsequent healing that varies logarithmically with time. Using all available borehole and surface records of more than 300 earthquakes that occurred between 1 January 2011 and 26 May 2011, we observe a reduction in the shear-wave velocity of about 5% in the upper few hundred meters after the Tohoku-Oki earthquake throughout northeastern Japan. The area of the velocity reduction is about 1,200 km wide, which is much wider than earlier studies reporting velocity reductions following other larger earthquakes. The reduction of the shear-wave velocity is an indication that the shear modulus, and hence the shear strength, is reduced over a large part of Japan.

1. Introduction

The Tohoku-Oki earthquake (M_W9.0) of 11 March 2011 is one of the largest earthquakes in recent times. The subduction of the Pacific Plate at a velocity of 8-8.5 cm/year [*DeMets et al.*, 2010] has resulted in many M_W 7+ earthquakes [*Miyazawa and Mori*, 2009]. Before and after the Tohoku-Oki earthquake, many smaller earthquakes occurred. We use ground motion excited by seismicity recorded by KiK-net (the strong-motion network operated by the National Research Institute for Earth Science and Disaster Prevention (NIED)) to estimate time-lapse changes of the shear-wave velocities in the shallow subsurface throughout northeastern Japan after the Tohoku-Oki earthquake.

To measure shear-wave velocities, we use *seismic interferometry*, developed over the last 10 years [*Claerbout*, 1968; *Trampert et al.*, 1993; *Lobkis and Weaver*, 2001; *Roux and Fink*, 2003; *Schuster et al.*, 2004; *Wapenaar*, 2004; *Bakulin and Calvert*, 2006; *Snieder et al.*, 2006] to determine the arrival time of waves that propagate between two sensors. This technique has been applied to earthquake data in various ways, such as measuring shear-wave velocity [e.g., *Snieder and Şafak*, 2006; *Sawazaki et al.*, 2009] and estimating deep subsurface structure [e.g., *Tonegawa et al.*, 2009; *Ruigrok et al.*, 2010].

In this paper, we present the time-lapse change of the near-surface shear-wave velocity throughout the east half of Japan after the Tohoku-Oki earthquake. First, we introduce the use of KiK-net data based on seismic interferometry and time interpolation. Then we show the waveforms of one KiK-net station retrieved by seismic interferometry. Finally, we present a shear-wave velocity-change map throughout northeastern Japan.

2. KiK-net

About 700 KiK-net stations are distributed across Japan [*Okada et al.*, 2004]. Each station has a borehole with three-component strong-motion seismographs at the bottom and top of the borehole. The sampling interval of KiK-net stations is 0.01 s.

We use all available KiK-net stations and seismicity from 1 January 2011 to 26 May 2011. The depths of borehole seismometers are between 100 m and 337 m (91% of the seismometers are at a depth less than 210 m). Magnitude of seismicity is between 2.8 and 9.0. The observed record, as used for seismic interferometry, ranges from 60 s to 300 s depending on the earthquake.

All the used events are at a depth greater than 7 km, which is a relatively large depth compared to the depth of the boreholes. The velocity in the near surface is much slower than it is at greater depths. Because of the depth of events and slow velocities in the near surface, the waves that travel between the sensors at each station propagate in the near-vertical direction. Hence we assume the incoming waves at the receivers are locally near-vertical plane waves. In this study, we use only the north-south horizontal component. Before the data processing, we apply a bandpass filter from 1 to 13 Hz for all earthquake data.

3. Computing methods

3.1. Deconvolution interferometry

Seismic interferometry is a technique to obtain the Green's function that accounts for wave propagation between two stations [*Claerbout*, 1968; *Lobkis and Weaver*, 2001; *Roux and Fink*, 2003; *Wapenaar*, 2004; *Bakulin and Calvert*, 2006; *Snieder et al.*, 2006]. Although the widest applied algorithm in seismic interferometry is based on cross correlation [e.g., *Claerbout*, 1968; *Wapenaar*, 2004; *Bakulin and Calvert*, 2004; *Schuster et al.*, 2004], we use the algorithm based on deconvolution [e.g., *Trampert et al.*, 1993; *Snieder and Şafak*, 2006; *Vasconcelos and Snieder*, 2008]. In deconvolution interferometry, we can suppress the complicated imprint of the structure (e.g., attenuation and scattering) incurred as the waves travel from the hypocenter to the borehole seismogram [*Snieder et al.*, 2009]. We denote the wavefield excited by an earthquake at location $\boldsymbol{s}$ that strikes the borehole receiver at location $\boldsymbol{r_b}$ by $u(\boldsymbol{r_b}, \boldsymbol{s}, \omega)$, and the wavefield recorded at the surface receiver at location $\boldsymbol{r_s}$ by $u(\boldsymbol{r_s}, \boldsymbol{s}, \omega)$ in the frequency domain. The deconvolved waveform is given by

$$D(\omega) = \frac{u(\boldsymbol{r_s}, \boldsymbol{s}, \omega)}{u(\boldsymbol{r_b}, \boldsymbol{s}, \omega)} \approx \frac{u(\boldsymbol{r_s}, \boldsymbol{s}, \omega) u^*(\boldsymbol{r_b}, \boldsymbol{s}, \omega)}{|u(\boldsymbol{r_b}, \boldsymbol{s}, \omega)|^2 + \epsilon}, \tag{1}$$

where $*$ is the complex conjugate and ϵ the regularization parameter that stabilized the deconvolution [*Snieder and Şafak*, 2006; *Mehta et al.*, 2007]. $D(\omega)$ is the frequency-domain waveform that propagates from the borehole sensor to the surface sensor [*Snieder and Şafak*, 2006; *Mehta et al.*, 2007; *Sawazaki et al.*, 2009; *Yamada et al.*, 2010]. We choose ϵ to be 1% of the average power spectrum of the wavefield at the borehole receiver because we find experimentally this is the smallest value of the regularization parameter that produces stable deconvolved wavefields.

3.2. Enhancing time resolution

Because the sampling time of KiK-net seismometers is larger than the changes in the travel time that we seek to measure, we interpolate the deconvolved waveforms and enhance the time resolution. We estimate the arrival time by selecting the three adjacent samples with the largest amplitude and quadratically interpolate between these points. We use the time of the maximum amplitude of the parabola thus obtained as the arrival time of the deconvolved wave. This makes it possible to measure the arrival time with a resolution better than the sampling time. We refer to this procedure as *quadratic interpolation*.

3.3. Estimating the angle of incidence

We compute the angle of the incoming wave at the borehole receiver by using one-dimensional ray tracing to confirm whether the wave propagating between the borehole and surface sensors propagates vertically. We use the velocity model of *Nakajima et al.* [2001] to determine the ray parameter p of the ray that connects each earthquake with the borehole sensor.The angle of incidence θ of the wave that propagates between the borehole and surface seismometers is then given by $\cos\theta = \sqrt{1 - p^2 v^2}$, where v is the average shear-wave velocity between these sensors as determined in this study. A bias in the velocity estimation due to non-vertical propagation depends on the deviation from $\cos\theta$ from its value for vertical incidence, $\cos 0° = 1$.

4. Determining shear-wave velocities throughout northeastern Japan

Figure 1a shows deconvolved waveforms of earthquakes between 1 January 2011 and 26 May 2011 for KiK-net station FKSH18 in the Fukushima prefecture at a distance of about 200 km from the epicenter of the Tohoku-Oki earthquake; Figure 1b shows the epicenters of the earthquakes that occurred during the periods before and after the event. The arrival times obtained by quadratic interpolation are shown with circles in Figure

1a. The average of $\cos\theta$ (see section 3.3) over the events between 1 January 2011 and 10 March 2011 is 0.984, while between 12 March 2011 to 26 May 2011 this average is equal to 0.980. This implies that the bias in the estimated shear-wave velocity is only about 2%, but this bias is virtually identical in the periods before and after the Tohoku-Oki earthquake. Hence changes in the pattern of seismicity before and after the main shock are not responsible of the change in the shear-wave velocity that we present. To enhance the data quality, we discard some data which has a low signal-to-noise ratio based on a visual inspection.

The travel time measured during the main shock of the Tohoku-Oki earthquake (the large magenta circle in Figure 1a) is significantly later than that from the other earthquakes. This indicates a reduction of the shear-wave velocity of about 22% during the shaking caused by the Tohoku-Oki event. Note also the delay of the waves in the early aftershocks indicated in red in Figure 1a. The delay of the waveforms after the Tohoku-Oki earthquake relative to the waveforms recorded before the event indicates that the shear waves propagate with a reduced shear-wave velocity after the Tohoku-Oki earthquake (Figure 1a).

Figure 2 depicts the travel-time change during the shaking caused by the Tohoku-Oki earthquake by applying short-time moving-window seismic interferometry to the seismogram, in which we deconvolve 20-s time windowed borehole and surface records at station FKSH18. Since the time window moves with 10-s intervals, the windows have a 10-s overlap. The main delay occurs at 30-40 s, and it is increasing while the shaking increases. After the strongest shaking (at 130 s), the travel times recover and are fairly constant.

Note that the delay, as well as the shear-wave velocity reduction, remains nonzero after 200 s compared to its values between 0-20 s. The velocity reduction at the time of strong shaking is likely to be influenced by several physical mechanisms including incipient liquefaction.

We compute the shear-wave velocity as a function of time from the interpolated travel times (the circles in Figure 1) using the known depth of the borehole. Figure 3 shows the shear-wave velocity estimated from each earthquake at station FSKH18. According to Figure 3, the velocity is reduced by almost 10% on the day after the Tohoku-Oki earthquake and the velocity recovers with about 5% in the 2 months after the earthquake. As shown by the orange curve in Figure 3, the shear-wave velocity after the Tohoku-Oki earthquake recovers logarithmically with time [*Dieterich*, 1972; *Vidale and Li*, 2003; *Schaff and Beroza*, 2004], $v_s(t) = a\ ln(t - t_0) + b$, where t_0 is the origin time of the Tohoku-Oki event, and t is time measured in days. We determine the parameters a and b by a linear least-squares fit of the data points shown by the red and blue dots in Figure 3. We exclude the data point of the Tohoku-Oki earthquake (the large magenta dot in Figure 3) in the estimation of the orange recovery curve in Figure 3 because the anomalously low velocity during the shaking by the Tohoku-Oki event may be caused by a complex physical mechanism mentioned above.

We compute the average of the deconvolved waveforms for station FKSH18 over the periods 1 January - 10 March (before) and 12 March - 26 May (after) in 2011 of Figure 1. These average waveforms are shown by the solid lines in Figure 4. The shapes of the average deconvolved waveforms before and after the Tohoku-Oki earthquake are similar, but the average waveform after the Tohoku-Oki earthquake is delayed. We also determine the average shear-wave velocities before and after the Tohoku-Oki earthquake from the interpolated travel times (the circles in Figure 4). The average velocity in the time interval before the Tohoku-Oki earthquake is 665 ± 7 m/s, and after the event it is 625 ± 14 m/s, hence the average velocity reduction is about 6%. The uncertainty of the velocities is determined from the standard deviations of the travel times over all events in each time interval.

It has been documented that the shear-wave velocity in the near surface may exhibit seasonal changes associated with changes in precipitation [*Sens-Schönfelder and Wegler*, 2006]. In order to investigate the influence of seasonal changes, we compute the mean shear-wave velocities in the periods 1 January - 10 March and 12 March - 26 May averaged over all years from 2000 to 2010. The corresponding waveforms are shown by the dashed lines in Figure 4. The mean velocity over the period 1 January - 10 March averaged from 2000-2010 is 664 ± 6 m/s, and the mean velocity for the interval 12 March - 26 May is 661 ± 6 m/s. The difference between these values is statistically not significant, and it is much smaller than the measured velocity change associated with the Tohoku-Oki earthquake.

We average the deconvolved waves at each KiK-net station over earthquakes recorded in the time intervals before (from 1 January 2011 to 10 March 2011) and after (from 12 March 2011 to 26 May 2011) the Tohoku-Oki event to determine the arrival times of the average deconvolved waveforms at each KiK-net station that are the travel time of the shear wave that propagates between the seismometers in the borehole and at the surface of each station. These times thus constrain the near-surface shear-wave velocity between the seismometers. We convert this travel time to the shear-wave velocity in the near-surface at each station, and following spatial interpolation [*Lawson*, 1984] of the velocities between stations, we obtain near-surface shear-wave velocity maps before (the upper-left map in Figure 5) and after (the middle map in Figure 5) the Tohoku-Oki earthquake. In order to reduce the uncertainty in the velocity estimates, we use only stations that recorded more than 3 earthquakes during both time intervals. The average $\cos\theta$ is greater than 0.975 but in the west side of the area $\cos\theta \approx 0.94 - 0.96$. These values are fairly constant in the time periods before and after the Tohoku-Oki earthquake. We use recorded data from 83 and 219 earthquakes, respectively, to create shear-wave velocity maps for the time intervals before and after the Tohoku-Oki earthquake. By subtracting the velocity measured before the main event from the velocity measured after the event, we obtain the map of the relative velocity change before and after the Tohoku-Oki earthquake shown in the lower-right map of Figure 5.

5. Discussion and Conclusions

It is known that large earthquakes can reduce seismic velocities close to the epicenter [e.g., *Li et al.*, 1998; *Vidale and Li*, 2003; *Schaff and Beroza*, 2004; *Wegler and Sens-Schönfelder*, 2007; *Brenguier et al.*, 2008; *Sawazaki et al.*, 2009; *Yamada et al.*, 2010]. As shown in Figure 5, the shear-wave velocity was reduced by about 5% after the Tohoku-Oki earthquake over an area in northeastern Japan about 1,200 km wide, which is much larger than the region of velocity reduction after the earthquakes reported in earlier studies. We also measured the mean shear-wave velocity reduction in these time intervals over the period from 2000 to 2010 of the whole area shown in the maps in Figure 5. The seasonal change in the shear-wave velocity is only 0.2%, which is much smaller than the velocity reduction observed following the Tohoku-Oki earthquake (see the lower-right map of Figure 5). We conclude that the shear-wave velocity reduction in Figure 5 is caused by the Tohoku-Oki earthquake. The area with reduced shear-wave velocity is delimited on the western side by the Median Tectonic Line (MTL) and the Itoigawa-Shizuoka Tectonic Line (ISTL) (the dashed black lines on the lower-right map in Figure 5). Because the number of recorded earthquakes at the west side of these tectonic lines is small, between 3 and 5, and the average of $\cos\theta$ is relatively low (around 0.94-0.96), the velocities in the western part are less reliable than those in other regions. The velocity reduction of Figure 5 does not correlate with the coseismic or postseismic displacements of the Tohoku-Oki earthquake [*Ozawa et al.*, 2011] because the velocity reduction is also influenced by variations in local geology.

With seismic interferometry, we extract the waves that propagate between the borehole and surface seismometers at KiK-net stations, and find a significant reduction of the near-surface shear-wave velocity after the Tohoku-Oki earthquake that recovers logarithmically with time. By applying this analysis to all available seismograms, we detect a reduction of the shear-wave velocity in the upper few hundred meters throughout the eastearn half of Japan. The shear-wave velocity is related to the shear modulus; hence the reduction of the shear-wave velocity over northeastern Japan implies that the Tohoku-Oki earthquake reduced the shear strength of the near surface throughout northeastern Japan.

Acknowledgments. We thank NIED for providing us with the KiK-net data. We are grateful to the editor, David Schaff, and one anonymous reviewer for suggestions, corrections, and discussions. Nori Nakata is grateful for the financial support from the Japan Society for the Promotion of Science (JSPS: 22-5857).

References

Bakulin, A., and R. Calvert, Virtual source: new method for imaging and 4D below complex overburden, *SEG Expanded Abstracts*, *23*, 112–115, 2004.

Bakulin, A., and R. Calvert, The virtual source method: Theory and case study, *Geophysics*, *71*(4), S1139–S1150, 2006.

Brenguier, F., M. Campillo, C. Hadziioannou, N. M. Shapiro, R. M. Nadeau, and E. Larose, Postseismic relaxation along the San Andreas Fault at Parkfield from continuous seismological observations, *Science*, *321*, 1478–1481, 2008.

Claerbout, J. F., Synthesis of a layered medium from its acoustic transmission response, *Geophysics*, *33*(2), 264–269, 1968.

DeMets, C., R. G. Gordon, and D. F. Argus, Geologically current plate motions, *Geophys. J. Int.*, *181*, 1–80, 2010.

Dieterich, J. H., Time-dependent friction in rocks, *J. Geophys. Res.*, *77*(20), 3690–3697, 1972.

Ito, T., T. Ikawa, S. Yamakita, and T. Maeda, Gently north-dipping Median Tectonic Line (MTL) revealed by recent seismic reflection studies, southwest Japan, *Tectonophysics*, *264*, 51–63, 1996.

Lawson, C. L., C^1 surface interpolation for scattered data on a sphere, *Rocky Mountain J. Math.*, *14*(1), 177–202, 1984.

Li, Y.-G., J. E. Vidale, K. Aki, F. Xu, and T. Burdette, Evidence of shallow fault zone strengthening after the 1992 M7.5 Landers, California, earthquake, *Science*, *279*, 217–219, 1998.

Lobkis, O. I., and R. L. Weaver, On the emergence of the Green's function in the correlations of a diffuse field, *J. Acoust. Soc. Am.*, *110*(6), 3011–3017, 2001.

Mehta, K., R. Snieder, and V. Graizer, Extraction of near-surface properties for a lossy layered medium using the propagator matrix, *Geophys. J. Int.*, *169*, 271–280, 2007.

Miyazawa, M., and J. Mori, Test of seismic hazard map from 500 years of recorded intensity data in Japan, *Bull. Seismol. Soc. Am.*, *99*(6), 3140–3149, doi:10.1785/0120080262, 2009.

Nakajima, J., T. Matsuzawa, A. Hasegawa, and D. Zhao, Three-dimensional structure of V_p, V_s, and V_p/V_s beneath northeastern Japan: Implications for arc magmatism and fluids, *J. Geophys. Res.*, *106*(B10), 21,843–21,857, 2001.

Okada, Y., K. Kasahara, S. Hori, K. Obara, S. Sekiguchi, H. Fujiwara, and A. Yamamoto, Recent progress of seismic observation networks in Japan — Hi-net, F-net, K-NET and KiK-net —, *Earth Planets Space*, *56*, 15–28, 2004.

Ozawa, S., T. Nishimura, H. Suito, T. Kobayashi, M. Tobita, and T. Imakiire, Coseismic and postseismic slip of the 2011 magnitude-9 Tohoku-Oki earthquake, *Nature*, doi: 10.1038/nature10227, 2011.

Roux, P., and M. Fink, Green's function estimation using secondary sources in a shallow wave environment, *J. Acoust. Soc. Am.*, *113*(3), 1406–1416, 2003.

Ruigrok, E., X. Campman, D. Draganov, and K. Wapenaar, High-resolution lithospheric imaging with seismic interferometry, *Geophys. J. Int.*, *183*, 339–357, doi:10.1111/j.1365-246X.2010.04724.x, 2010.

Sawazaki, K., H. Sato, H. Nakahara, and T. Nishimura, Time-lapse changes of seismic velocity in the shallow ground caused by strong ground motion shock of the 2000 western-Tottori earthquake, Japan, as revealed from coda deconvolution analysis, *Bull. Seismol. Soc. Am.*, *99*(1), 352–366, 2009.

Schaff, D. P., and G. C. Beroza, Coseismic and postseismic velocity changes measured by repeating earthquakes, *J. Geophys. Res.*, *109*, B10,302, doi:10.1029/2004JB003011, 2004.

Schuster, G. T., J. Yu, J. Sheng, and J. Rickett, Interferometric/daylight seismic imaging, *Geophys. J. Int.*, *157*, 838–852, 2004.

Sens-Schönfelder, C., and U. Wegler, Passive image interferometry and seasonal variations of seismic velocities at Merapi Volcano, Indonesia, *Geophys. Res. Lett.*, *33*, L21,302, 2006.

Snieder, R., and E. Şafak, Extracting the building response using seismic interferometry: Theory and application to the Millikan library in Pasadena, California, *Bull. Seismol. Soc. Am.*, *96*(2), 586–598, 2006.

Snieder, R., K. Wapenaar, and K. Larner, Spurious multiples in seismic interferometry of primaries, *Geophysics*, *71*(4), SI111–SI124, 2006.

Snieder, R., M. Miyazawa, E. Slob, I. Vasconcelos, and K. Wapenaar, A comparison of strategies for seismic interferometry, *Surveys in Geophysics*, *30*(10), 503–523, 2009.

Tonegawa, T., K. Nishida, T. Watanabe, and K. Shiomi, Seismic interferometry of teleseismic S-wave coda retrieval of body waves: an application to the Philippine Sea slab underneath the Japanese Islands, *Geophys. J. Int.*, *178*, 1574–1586, doi:10.1111/j.1365-246X.2009.04249.x, 2009.

Trampert, J., M. Cara, and M. Frogneux, SH propagator matrix and Q_s estimates from borehole- and surface- recorded earthquake data, *Geophys. J. Int.*, *112*, 290–299, 1993.

Vasconcelos, I., and R. Snieder, Interferometry by deconvolution, Part 1 - Theory for acoustic waves and numerical examples, *Geophysics*, *73*(3), S115–S128, 2008.

Vidale, J. E., and Y.-G. Li, Damage to the shallow Landers fault from the nearby Hector Mine earthquake, *Nature*, *421*, 524–526, 2003.

Wapenaar, K., Retrieving the elastodynamic Green's function of an arbitrary inhomogeneous medium by cross correlation, *Phys. Rev. Lett.*, *93*, 254–301, 2004.

Wegler, U., and C. Sens-Schönfelder, Fault zone monitoring with passive image interferometry, *Geophys. J. Int.*, *168*, 1029–1033, 2007.

Yamada, M., J. Mori, and S. Ohmi, Temporal changes of subsurface velocities during strong shaking as seen from seismic interferometry, *J. Geophys. Res.*, *115*, B03,302, 2010.

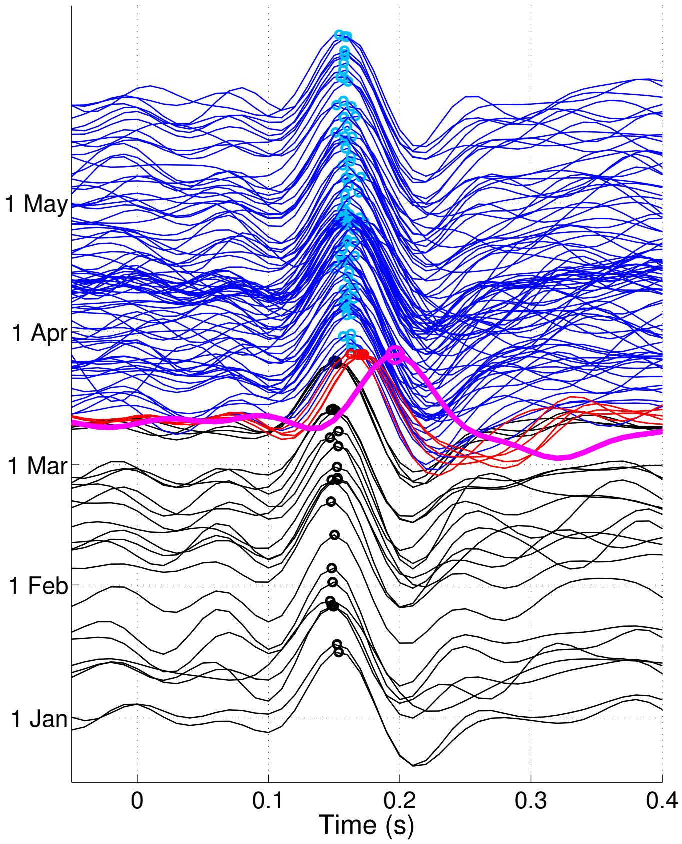

(a)

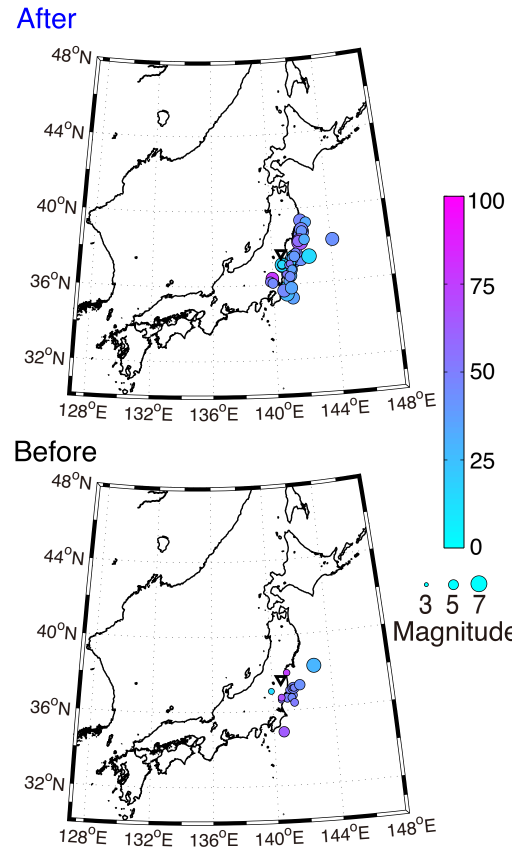

(b)

Figure 1. (a) Deconvolved waveforms of individual earthquakes from 1 January 2011 to 26 May 2011 at station FKSH18. This station recorded 25 earthquakes from 1 January 2011 to 10 March 2011 (black curves), the Tohoku-Oki earthquake of 11 March 2011 (magenta thick curve), 5 other earthquakes on 11 March 2011 (red curves), and 96 earthquakes from 12 March 2011 to 26 May 2011 (blue curves). Circles, marked by the same color as the waveforms (blue replaces cyan), represent the interpolated arrival times of waves. The waveforms are ordered by the origin times of earthquakes in the vertical axis. (b) Epicenters of two time intervals: 1 January 2011 to 10 March 2011 and 12 March 2011 to 26 May 2011. The size of each circle indicates the magnitude of each earthquake and the color denotes the depth. The white triangle points to the location of station FKSH18.

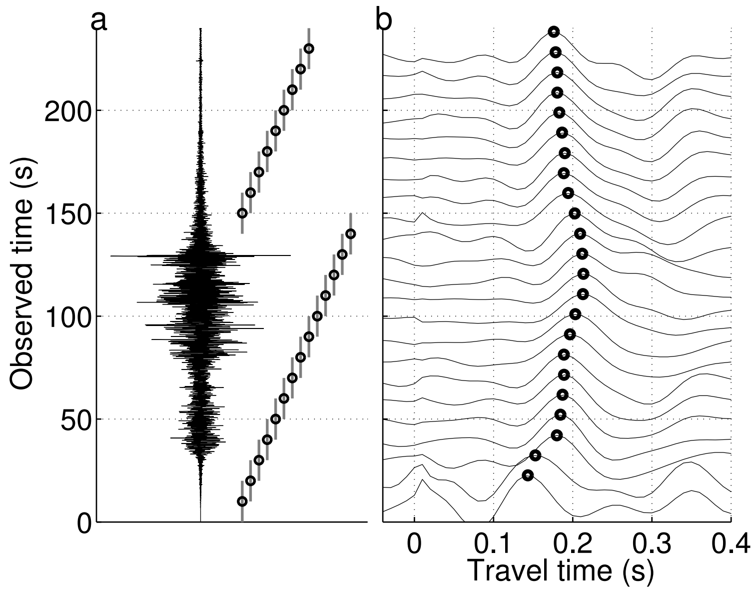

Figure 2. Short-time moving-window seismic interferometry of the ground motion caused by the Tohoku-Oki earthquake. (a) The earthquake record observed at the north-south horizontal component borehole seismometer of station FKSH18. Gray bars indicate the 20-s time windows for seismic interferometry with 10-s overlap. Black circles are the center of each window. (b) Deconvolved waveforms of each time window. Each waveform is aligned with the center time of the employed time window. Black circles illustrate the interpolated arrival times.

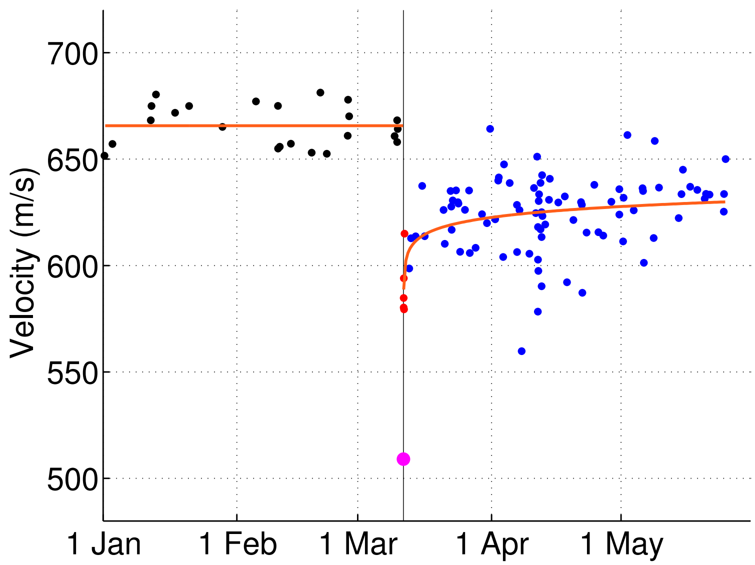

Figure 3. Shear-wave velocity variations in the upper 100 m at station FKSH18. By using the arrival times of waves (the circles in Figure 1), we compute the velocity variations from 1 January 2011 to 26 May 2011. The color of each dot is the same as in Figure 1. Black vertical line indicates the origin time of the Tohoku-Oki earthquake. Orange line depicts the average velocity (before the Tohoku-Oki earthquake) and the logarithm curve determined by least-squares fitting of the velocity after the earthquake. We do not include the Tohoku-Oki earthquake data point (magenta dot) in the data fit.

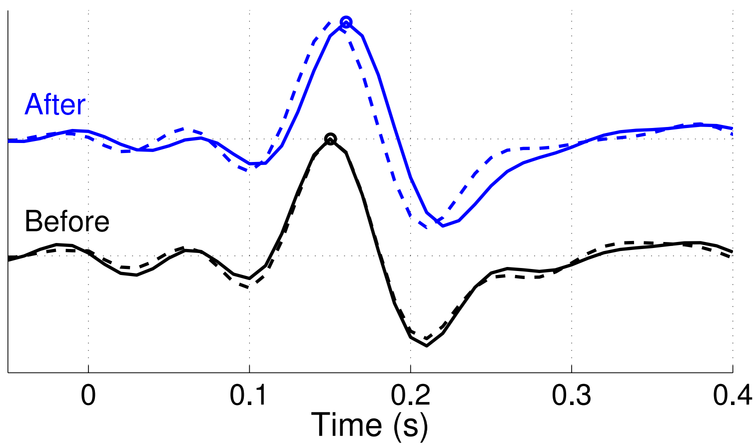

Figure 4. Averaged waveforms of Figure 1 before (from 1 January 2011 to 10 March 2011; black solid curve) and after (from 12 March 2011 to 26 May 2011; blue solid curve) the Tohoku-Oki earthquake at station FKSH18. Circles denote the interpolated arrival times of averaged waves. Black and blue dashed curves represent the averaged waveforms from 1 January to 10 March and from 12 March to 26 May over 11 years (from 2000 to 2010), respectively.

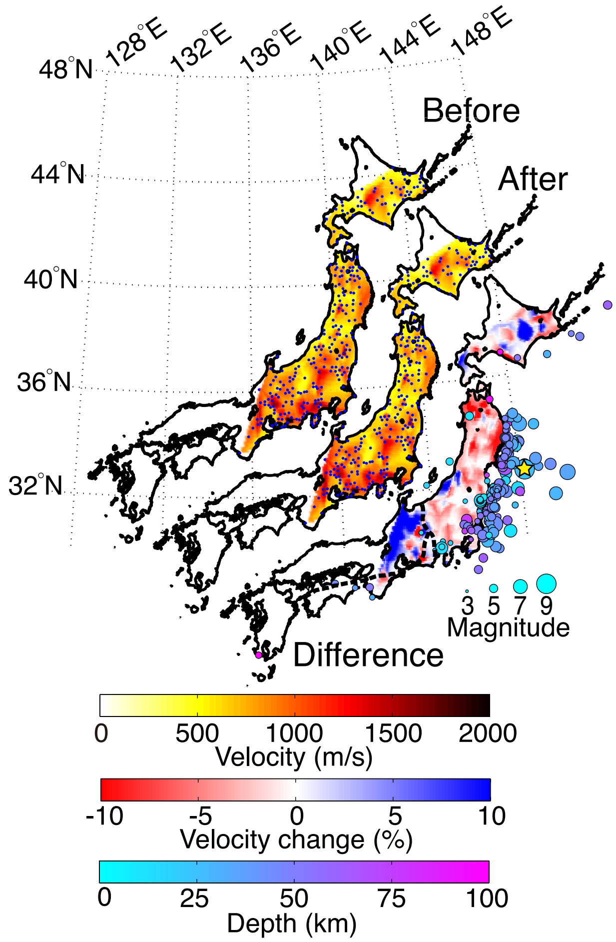

Figure 5. Shear-wave velocities estimated from deconvolved waveforms before (upper-left) and after (middle) the Tohoku-Oki earthquake. Blue dots on these two maps show the KiK-net stations used in this study. The map on the lower-right gives the relative change in shear-wave velocity before and after the event. The longitude and latitude belong to the map in the upper-left. Locations and magnitude of the earthquakes from 1 January 2011 to 26 May 2011 are shown as circles, relative to the map on the lower-right. The size of each circle indicates the magnitude of each earthquake and the color represents the depth. The yellow star denotes the location of the Tohoku-Oki earthquake. The dashed black lines show the locations of MTL and ISTL [*Ito et al.*, 1996].